Beam Direction-Based Modulation for Millimeter-Wave Communication Systems: Design and Optimization

Ke Jiang, Ping Yang, Marco Di Renzo, Yue Xiao, Shaoqian Li, Wei Xiang

Beam Direction-Based Modulation for Millimeter-Wave Communication Systems: Design and Optimization

Ke Jiang, Ping Yang, Marco Di Renzo, *Fellow, IEEE*, Yue Xiao, *Member, IEEE*, Shaoqian Li, *Fellow, IEEE*, and Wei Xiang, *Senior Member, IEEE*

***Abstract*—In this paper, we investigate a novel beam direction-based modulation transmit scheme for millimeter-wave (mmWave) communication systems equipped with distributed antennas, and propose an enhanced space-domain index modulation (ESDIM) scheme, in which the number of beamforming directions (BDs) for transmitting information bits can be one or two. The ESDIM system jointly utilizes the combination of the index of BDs and signal constellations to transmit information bits, in which one or two beam directions are considered. In addition, we propose power allocation (PA) aided schemes for ESDIM to further improve the system reliability by reducing the system symbol error rate (SER), where three constraints to the transmit power for beamforming are investigated. To be specific, a total transmit power constraint (TTPC) and two per-beamforming power constraints (PBPC) are considered. We first propose a suboptimal PA algorithm for the TTPC-PA aided ESDIM scheme using a powerful solver based on advanced algebra theories, which only considers the PA aspects for a given selected beamforming pair. Then, we extend the TTPC-PA aided scheme to the average per-beamforming power constraint (APBPC)-PA aided scheme and the strict per-beamforming power constraint (SPBPC)-PA aided scheme. Simulation results show that the proposed schemes improve the system SER performance compared to other existing counterparts.**

***Index Terms*—Index modulation, millimeter-wave communication, power allocation, total transmit power constraint, per-beamforming power constraint.**

I. Introduction

MILLIMETER wave (mmWave) communications have attracted a lot of attention and are promising enabling techniques for the fifth generation (5G) and beyond wireless networks, thanks to their capability of providing massive connectivity and ample spectrum [1], [2], [3].

It is well known that the high path loss is one of the shortcomings of mmWave communications. Some researchers have tried to circumvent this by combining mmWave communications with space-domain index modulation (SDIM) [4]–[8]. For example, the authors of [4] introduced the concept of SDIM in mmWave systems, where the space shift keying (SSK) scheme was studied in line-of-sight (LOS) conditions. It was shown that SDIM is a promising scheme, which can strike a good trade-off among different performance metrics, such as the bit error ratio (BER), the complexity and hardware cost. Moreover, based on the concept of SSK modulation, the space-time shift keying (STSK) scheme was proposed and was combined with orthogonal frequency division multiplexing for application to mmWave systems, in order to achieve higher data throughput and better BER performance [5], [6], [7], [8]. In addition, by jointly leveraging analog and hybrid beamforming for mmWave systems [9], [10], [11], [12], another scheme, termed spatial scattering modulation (SSM), was proposed and was generalized for application to mmWave communications. Specifically, SSM modulates some information bits on the spatial directions of the scattering clusters in the angular domain.

In the existing contributions, as a representative of antenna activation based SDIM (AA-SDIM), spatial modulation (SM) based mmWave communication schemes have attracted much attention. In [21] and [22], SM-mmWave schemes were proposed for application to high-speed railway wireless communications and indoor communications at 60 GHz, respectively. More recently, variants of SM, such as generalized spatial modulation (GSM) [18], [19], [23], [24], [25], quadrature spatial modulation (QSM) [26], [27], and receive spatial modulation (RSM) [28], [29], were investigated to improve the performance of mmWave communication systems. In [23], specifically, an array of analog beamformers was employed, consisting of several weighted multiple transmit antennas. The proposed GSM-based scheme is capable of maintaining high capacity with a reduced number of radio frequency (RF) chains. The authors of [24] studied the system capacity and the symbol error probability of GSM over measured mmWave indoor channels at 60 GHz, as well as the impact of non-LOS components on the system

Manuscript received 2 December 2021; revised 4 June 2022 and 28 September 2022; accepted 20 October 2022. Date of publication 27 October 2022; date of current version 14 March 2023. This work was supported in part by the National Key R&D Program of China under Grant 2020YFB1807203, in part by the National Science Foundation of China under Grant 61876033, and in part by the National Science Foundation of China under Grant U19B2014. The review of this article was coordinated by Prof. Yong Liang Guan. *(Corresponding author: Ping Yang.)*

Ke Jiang, Ping Yang, Yue Xiao, and Shaoqian Li are with the National Key Laboratory of Science and Technology on Communications, University of Electronic Science and Technology of China, Sichuan 611731, China (e-mail: jiangke@std.uestc.edu.cn; yang.ping@uestc.edu.cn; xiaoyue@uestc.edu.cn; lsq@uestc.edu.cn).

Marco Di Renzo is with the Université Paris-Saclay, CNRS, CentraleSupélec, Laboratoire des Signaux et Systèmes, 3 Rue Joliot-Curie, 91192 Gif-sur-Yvette, France (e-mail: marco.direnzo@lss.supelec.fr).

Wei Xiang is with the School of Engineering and Mathematical Sciences, La Trobe University, Melbourne, VIC 3086, Australia (e-mail: w.xiang@latrobe.edu.au).

error performance. In high-mobility mmWave channels, where the channel coefficients change rapidly, a large-scale differential detector aided GSM scheme was proposed in [25], which can achieve a maximum transmission rate of 16 bps/Hz. In [26], QSM was firstly employed in mmWave communications, and a detailed analysis of the mutual information and achievable capacity of mmWave-QSM was presented. Besides, QSM was analyzed to achieve green and secure mmWave communications by using a frequency modulated diverse retrospective array in [27]. The proposed scheme was shown to improve the spectral efficiency at a low complexity and without requiring channel state information. RSM, also referred to as precoding-aided (or preprocessing-aided) spatial modulation (PSM), was employed for mmWave communications as well. In [28], RSM and analog beamforming were jointly employed by the transmitter to achieve beamforming gains and reduce the computational complexity. The authors of [29] applied RSM in indoor LOS mmWave channels, and proved that imposing the orthogonality on the channel matrix can minimize the symbol error rate of mmWave-RSM.

Besides AA-SDIM for mmWave communications, another type of SDIM for mmWave communications is beam direction based SDIM (BD-SDIM) [13], [14], [15], [16], [17], [18], [19], [20]. In [13], a novel scheme similar to SSM, which is referred to as virtual space modulation (VSM), was proposed. VSM is able to achieve significant signal-to-noise ratio (SNR) improvement in mmWave channels. In order to enhance the multiplexing gains and the spectral efficiency in mmWave systems with a limited number of radio-frequency (RF) chains at the transmitter and receiver, generalized beamspace modulation (GBM) was proposed and investigated in [14], [15], [16], [17]. In [18], a hybrid precoding technique was integrated into a GSM-aided mmWave MIMO system in an attempt to improve the system throughput, and an accurate approximation for the spectral efficiency was derived. Similar to [18], a hybrid analog and digital precoding scheme was proposed to maximize the spectral efficiency of GSM-based mmWave systems, and a lower bound for the achievable spectral efficiency was derived in [19]. The authors of [20] proposed a novel SDIM scheme, which is referred to as beam index modulation, which uses analog beamforming, and requires a lower hardware complexity than its SSM counterpart.

Furthermore, link adaption aided SM-based mmWave communication schemes were proposed in [30], [31], [32], [33]. Specifically, the receive antenna selection (RAS)-aided SM was proposed for application to mmWave systems in [30]. Therein, two RAS algorithms based on maximizing the capacity and minimizing the bit error rate were proposed. The authors of [31] proposed a scheme for uplink mmWave communications, which adaptively selects the spatial signatures of the transmitted signal to mitigate the channel fading, hence reducing the system error rate effectively. In addition, the authors of [32] applied the space-domain index modulation scheme to mmWave cloud radio access networks with distributed antennas, so as to achieve a better system reliability. Also, they proposed a PA algorithm to enhance the symbol error ratio (SER). In [33], the same authors extended the scheme in [32] to a generalized case with arbitrary beam direction combinations, and optimized the signal transmission using multi-domain modulations. Additional research works on mmWave cloud radio access networks include [34], [35], [36], [37]. Specifically, the authors of [34] considered downlink multiuser transmissions for mmWave cloud radio access networks and proposed two special mobile equipment association scenarios, including the best channel participation (BCP) and the nearest neighbor participation (NNP). The authors of [35] investigated cooperative mmWave multiuser communications and proposed a beamforming method to improve the energy efficiency. An adaptive array design based on the channel state of line-of sight (LoS) or non-line-of-sight (NLoS) links was proposed for mmWave cloud radio access networks in [36]. This scheme encompasses a fully connected and a sub-array-connected architectures. The authors of [37] analyzed the spatial multiplexing gains of mmWave distributed systems under the assumption of an infinite number of antennas at the subarrays and assuming a fixed transmit power.

Motivated by the fact that the performance of mmWave communication systems highly depends on the severe path loss and LoS blockage, and that few existing works have considered multiple-mode BD-SDIM based distributed antenna systems with link adaptation in the mmWave frequency band, we propose a joint design beamforming and conventional signal constellations to improve the reliability of exiting SDIM schemes.

Specifically, the main contributions of this paper are as follows:

- We propose a novel enhanced SDIM (ESDIM) scheme for mmWave communications, which jointly utilizes the combinations of beamforming directions (BDs) and signal constellations to improve the reliability of mmWave systems with distributed antennas. By taking advantage of the multiple combinations of BDs and multiple signal constellations, the proposed ESDIM-based scheme is shown to improve the SER performance;
- Based on the proposed ESDIM-based scheme, we investigate PA schemes to further improve the system reliability. We first propose a suboptimal PA algorithm and obtain the PA matrix given a total transmit power constraint (TTPC). Then, we derive closed-form solutions for the suboptimal PA matrix by using advanced algebra theories;
- We extend the TTPC-PA aided scheme for application to the ESDIM system, and consider the PA problem with stricter power constraints, i.e., the average per-beamformer power constraint (APBPC) and the strict per-beamformer power constraint (SPBPC) for each activated BD. Comprehensive simulations for different system configurations are performed, in order to compare the three considered PA schemes. The simulation results show that the proposed ESDIM scheme and the PA-aided schemes improve the system reliability.

Notations: Boldface capital and lowercase symbols represent matrices and column vectors, respectively. $(\cdot)^T$, $(\cdot)^H$, and $||\cdot||$ denote transpose, Hermitian transpose, Frobenius norm, respectively. $|\cdot|$ denotes the magnitude of a complex number. The operator $diag(\cdot)$ applied to a vector returns a square matrix

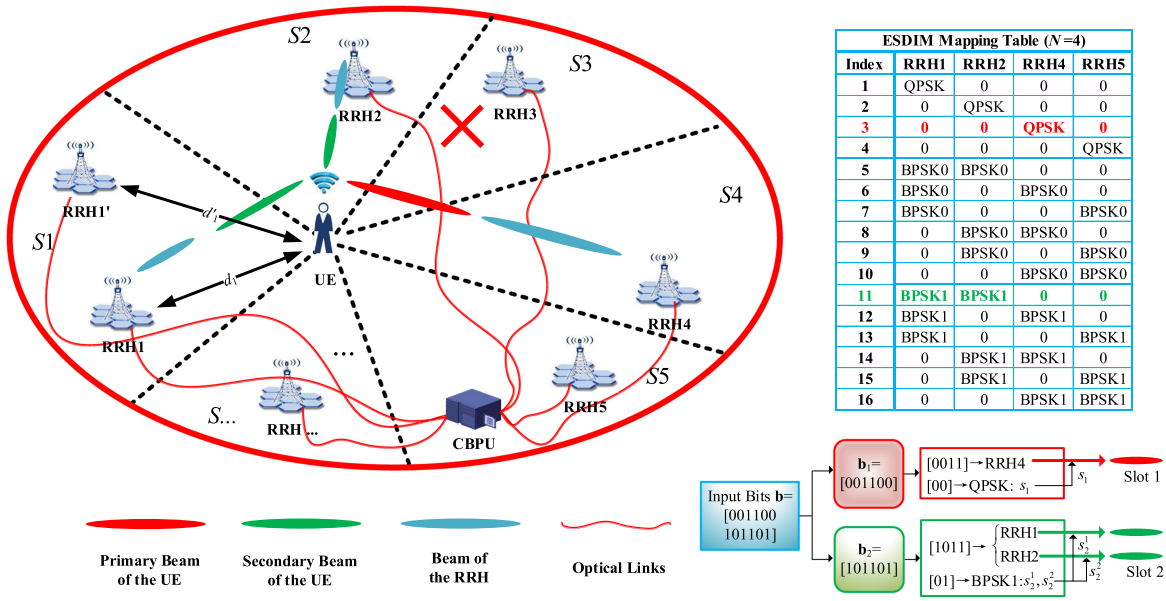

ESDIM Mapping Table (N=4)

Index	RRH1	RRH2	RRH4	RRH5
1	QPSK	0	0	0
2	0	QPSK	0	0
3	0	0	QPSK	0
4	0	0	0	QPSK
5	BPSK0	BPSK0	0	0
6	BPSK0	0	BPSK0	0
7	BPSK0	0	0	BPSK0
8	0	BPSK0	BPSK0	0
9	0	BPSK0	0	BPSK0
10	0	0	BPSK0	BPSK0
11	BPSK1	BPSK1	0	0
12	BPSK1	0	BPSK1	0
13	BPSK1	0	0	BPSK1
14	0	BPSK1	BPSK1	0
15	0	BPSK1	0	BPSK1
16	0	0	BPSK1	BPSK1

Fig. 1. Illustrations of the ESDIM-based mmWave system with distributed antennas, and the ESDIM mapping. The coverage area is divided into $\lfloor \frac{2\pi}{\theta} \rfloor$ parts and the RRH in each sector forwards signals to the CBPU for centralized processing.

with the vector elements along the diagonal. $E(\cdot)$ denotes the expectation operator and $tr(\cdot)$ denotes the trace operator (sum of the diagonal elements). $Re\{z\}$ is the real part of the complex number z, and z^* is the complex conjugate of z. C_n^k is the number of combinations of selecting k out of n numbers. $|\mathbb{E}|$ is the cardinality of the set $\mathbb{E}$.

II. System Model

A. Mmwave System with Distributed Antennas

Consider a mmWave communication system with distributed antennas, as shown in Fig. 1, where the user equipment (UE) is surrounded and served by several remote radio heads (RRHs). Based on the sectorized beamforming model in [38], and denoting by θ the beamwidth of the UE, the circular coverage area can be divided into $\lfloor \frac{2\pi}{\theta} \rfloor$ sectors, each of which may contain multiple RRHs.

Since the performance of mmWave communications is mainly determined by the link blockage and the path loss between the transmitter and receiver, the small-scale fading is ignored in this paper [39]. In addition, inspired by [39], [40], [41], only RRHs with LoS links with the UE are considered. Therefore, there are $N_0 \leq \lfloor \frac{2\pi}{\theta} \rfloor$ possible candidate RRHs. In the sectors where multiple LoS RRHs are present, only the RRH with the shortest distance to the UE is considered. In Fig. 1, consider, for example, $RRH1$ and $RRH1'$ in the i-th sector ($S1$). Since $d_1' > d_1$, $RRH1$ is selected as the candidate RRH for $S1$. Considering for example, on the other hand, $RRH3$ in $S3$, it is not selected as a candidate RRH, since the LoS link with the UE is blocked by some obstacles. The selection of the candidate RRHs from all the available ones is discussed in further text. The UE transmits information bits to the RRHs, which forward the received signals to the central baseband process unit (CBPU) via an optical link. At the CBPU, the signals from each RRH are processed jointly. The UE and RRHs are equipped with an array of N_t transmit and N_r receive antennas, respectively.

B. SDIM Communication Scheme

In the SDIM-based mmWave scheme with only one transmit mode [32], [33], the UE transmits information bits by jointly utilizing one BD and traditional amplitude and phase modulation (APM) symbols. The first portion of the transmit bits is mapped to a space vector, which is used to select the candidate RRH, and the remaining bits are mapped to an APM symbol. In each time slot, the UE chooses one of the surrounding $N \leq N_0$ LoS RRHs (since some RRHs may have a higher path loss than others, they are not selected) and steers its main lobe towards the selected RRH and transmits APM symbols. Specifically, joint exploiting APM and BDs in SDIM is realized by using a phased antenna array, as shown in Fig. 2. The angles of arrival at the selected RHHs are controlled by using predefined phase shift vectors and the RRHs can only receive signals from some predefined directions. The phased antenna array of the UE is optimized to control the directions of the transmitted signals (beams) towards the predefined directions. Further details are given in Section II-C. In the SDIM scheme, the phased antenna array of the UE is used to control the transmit BDs and to transmit the APM symbol.

C. ESDIM Communication Scheme

Based on the SDIM scheme in Section II-B, the UE steers its main lobe only towards one RRH in each time slot. In the proposed ESDIM, on the other hand, information symbols can be transmitted to one RRH or two RRHs simultaneously.

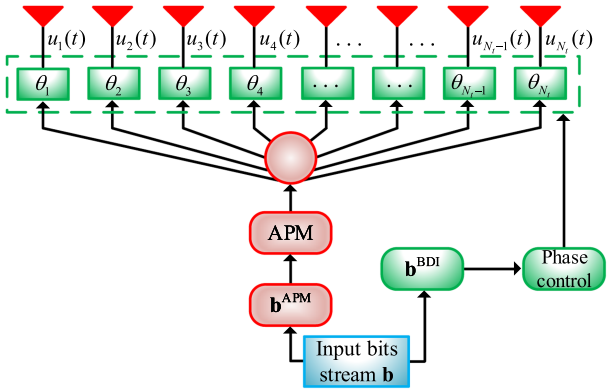

Fig. 2. An example of the phased antenna array at the UE to realize the combinations of BDs and APM.

Specifically, as shown in Fig. 1, one or two BDs of the UE are exploited to convey information bits that are determined by the first $\log_2(N)$ information bits. On the other hand, the remaining $\log_2(N_s)$ bits are used to select one primary N_s-ary APM constellation symbol or two secondary $N_s/2$-ary APM symbols. The UE steers its main lobes towards the RRHs selected by the first $\log_2(N)$ bits. Thus, the total transmission rate of the proposed system is

$$R_b = \log_2 N_s + \lfloor \log_2 \left(\mathcal{C}_N^1 + 2\mathcal{C}_N^2 \right) \rfloor \quad \text{bits/symbol.} \tag{1}$$

To illustrate the proposed encoding principle, let us consider an example. The UE is surrounded by $N = 4$ candidate RRHs, each of them is responsible for receiving information symbols for its assigned area. Quadrature phase shift keying (QPSK) modulation is utilized as the primary signal constellation. Consider the input information bit stream $\mathbf{b} = [001100101101]$. First, it is split into two groups $\mathbf{b}_1 = [001100]$ and $\mathbf{b}_2 = [101101]$. The bits in the groups $\mathbf{b}_1$ and $\mathbf{b}_2$ are further split into two parts, respectively. More specifically, group $\mathbf{b}_1$ is split into the beamforming direction index (BDI) $\mathbf{b}_1^{\mathrm{BDI}} = [0011]$ and the APM symbols bits $\mathbf{b}_1^{\mathrm{APM}} = [00]$. By exploiting the phased antenna array illustrated in Fig. 2, $\mathbf{b}_1^{\mathrm{BDI}}$ is used to configure the phase shifters and to beamform the signal to the candidate $RRH4$, and $\mathbf{b}_1^{\mathrm{APM}}$ is mapped to the symbol $s_1^1 = (1+i)/\sqrt{2}$. Accordingly, the UE steers its main lobe towards the 3 rd candidate RRH (i.e., $RRH4$) and transmits the symbol s_1^1.

Similarly, the bit group $\mathbf{b}_2 = [101101]$ is spilt into the BDI part $\mathbf{b}_2^{\mathrm{BDI}} = [1011]$ and the APM part $\mathbf{b}_2^{\mathrm{APM}} = [01]$. According to the mapping rules in Fig. 1, $\mathbf{b}_2^{\mathrm{BDI}}$ is used to select the transmit combination of two BDs and the secondary signal constellation BPSK1. This encoding scheme can be extended to transmit two APM symbols, where $\mathbf{b}_2^{\mathrm{BDI}}$ is used to configure the phased antenna array to steer two beams towards $RRH1$ and $RRH2$ and to transmit two BPSK1 symbols simultaneously. As shown in Fig. 1, the bits $\mathbf{b}_2^{\mathrm{APM}}$ are mapped to two BPSK1 symbols $s_2^1 = i/\sqrt{2}$ and $s_2^2 = -i/\sqrt{2}$, where BPSK1 is the rotated version of the ordinary BPSK with a rotation angle of $\frac{\pi}{2}$. In this paper, the ordinary BPSK modulation is denoted as BPSK0.

Based on this example, the generalized received baseband signal at each RRH can be formulated in one of the following two forms:

- Form 1: Only one candidate RRH is selected:

$$\begin{cases} y_i = \sqrt{GML_i} s_{n_0}^1 + z_i \\ y_j = \sqrt{GmL_j} s_{n_0}^1 + z_j \\ s_{n_0}^1 \in \mathbb{S}_1, i \neq j, \end{cases}, \ 1 \leq n_0 \leq N_s, \tag{2}$$

  where M and m are the beamforming main lobe and side lobe gains, respectively; G is the antenna gain of the RRH; y_i is the received signal at the i-th RRH, which is the only RRH towards which the UE steers its main lobe; y_j $(i \neq j)$ is the received signal at the j-th RRH; $s_{n_0}^1$ $(1 \leq n_0 \leq N_s)$ is the baseband symbols drawn from an N_s-ary APM constellation set $\mathbb{S}_1$; L_i and L_j denote the path loss of the i-th and j-th RRHs; z_i and $z_j \sim \mathcal{N}(0, N_0)$ denote the additive White Gaussian noises (AWGN) at the i-th and j-th RRHs, respectively.
- Form 2: Two candidate RRHs are selected simultaneously:

$$\begin{cases} y_a = \sqrt{GML_a} s_{n_1}^2 + \sqrt{GmL_a} s_{n_2}^2 + z_a \\ y_b = \sqrt{GmL_b} s_{n_1}^2 + \sqrt{GML_b} s_{n_2}^2 + z_b \\ y_c = \sqrt{GmL_c} s_{n_1}^2 + \sqrt{GmL_c} s_{n_2}^2 + z_c \\ s_{n_1}^2, s_{n_1}^2 \in \mathbb{S}_2, a \neq b \neq c, \end{cases}, \tag{3}$$

  where y_a and y_b represent the received signal at the a-th and b-th RRHs, respectively, towards which the UE steers its two main lobes; y_c is the received signal at the c-th RRH; $s_{n_1}^2$, $s_{n_2}^2$ $(1 \leq n_1, n_2 \leq N_s/2)$ are the baseband symbols drawn from an $N_s/2$-ary APM constellation set $\mathbb{S}_2$ (or $\mathbb{S}_3$); L_a, L_b and L_c denote the path loss of the a-th, b-th and c-th RRHs; z_a, z_b and $z_c \sim \mathcal{N}(0, N_0)$ denote the AWGN at the a-th, b-th and c-th RRHs, respectively.

The selected RRHs first convert the received radio-frequency signals into baseband signals, and then forward the baseband signals to the CBPU. Then, the received signals of the CBPU can be expressed as

$$\mathbf{y} = [y_1, y_2, \ldots, y_N]^T = \begin{cases} \mathbf{h}_i s_{n_0}^1 + \mathbf{z}, \\ \mathbf{h}_a s_{n_1}^2 + \mathbf{h}_b s_{n_2}^2 + \mathbf{z}, a \neq b, \end{cases} \tag{4}$$

where

$$\mathbf{h}_n = \sqrt{G} \left[\sqrt{mL_1}, \ldots, \sqrt{ML_n}, \ldots, \sqrt{mL_N} \right]^T, \ n = i, a, b \tag{5}$$

is the equivalent channel vector, and $\mathbf{z} = [z_1, z_2, \ldots, z_N]^T$ is the equivalent AWGN vector. Define $\mathbf{H} = [\mathbf{h}_1, \mathbf{h}_2, \ldots, \mathbf{h}_N]^T$, then (4) can be rewritten as

$$\mathbf{y} = [y_1, y_2, \ldots, y_N]^T = \begin{cases} \mathbf{H}\mathbf{e}_i s_{n_0}^1 + \mathbf{z}, \\ \mathbf{H} \left(\mathbf{e}_a s_{n_1}^2 + \mathbf{e}_b s_{n_2}^2 \right) + \mathbf{z}, \end{cases} \tag{6}$$

where

$$\mathbf{H} = \begin{pmatrix} \sqrt{GML_1} & \sqrt{GmL_1} & \cdots & \sqrt{GmL_1} \\ \sqrt{GmL_2} & \sqrt{GML_2} & \cdots & \sqrt{GmL_2} \\ \vdots & \vdots & \ddots & \vdots \\ \sqrt{GmL_N} & \sqrt{GmL_N} & \cdots & \sqrt{GML_N} \end{pmatrix}, \tag{7}$$

is the equivalent $N \times N$ channel matrix [33], $\mathbf{e}_i$, $\mathbf{e}_a$ and $\mathbf{e}_b$ are the i-th, a-th and b-th columns of the identity matrix $\mathbf{I}_N$,

respectively. Thus, the centralized maximum likelihood (ML) detector can be expressed as

$$\begin{cases}\left[\hat{i},\hat{n}_0\right]=\arg\min\limits_{i,n_0}\left\|\mathbf{y}-\mathbf{H}\mathbf{e}_i s^1_{n_0}\right\|^2,\\ \left[\hat{a},\hat{b},\hat{n}_1,\hat{n}_2\right]=\arg\min\limits_{a,b,n_1,n_2}\left\|\mathbf{y}-\mathbf{H}\left(\mathbf{e}_a s^2_{n_1}+\mathbf{e}_b s^2_{n_2}\right)\right\|^2.\end{cases} \tag{8}$$

Let us denote $\mathbf{x}_1=\mathbf{e}_i s^1_{n_0}$, $\mathbf{x}_2=\mathbf{e}_a s^2_{n_1}+\mathbf{e}_b s^2_{n_2}$ for $\forall i$, a, b, n_0, n_1, n_2. The pairwise error probability of estimating $\tilde{\mathbf{x}}$ as the transmitted $\mathbf{x}$ is given by

$$P_e\left(\mathbf{x}\to\tilde{\mathbf{x}}\right)=Q\left(\sqrt{\frac{\left\|\mathbf{H}\left(\mathbf{x}-\tilde{\mathbf{x}}\right)\right\|^2}{N_0}}\right),\ \mathbf{x},\tilde{\mathbf{x}}\in\left\{\mathbf{x}_1,\mathbf{x}_2\right\}, \tag{9}$$

where $Q(x)=\int_x^{+\infty}e^{-t^2/2}dt/\sqrt{2\pi}$ is the Q-function. So, the SER of the system is bounded by

$$P_{\text{SER}}\le\frac{1}{2^{M+N}}\sum_{\mathbf{x}\neq\tilde{\mathbf{x}}}Q\left(\sqrt{\frac{\left\|\mathbf{H}\left(\mathbf{x}-\tilde{\mathbf{x}}\right)\right\|^2}{N_0}}\right). \tag{10}$$

According to (10), the SER is mainly determinated by the following term

$$d_{\min}=\min_{\substack{\mathbf{x},\tilde{\mathbf{x}}\in\{\mathbf{x}_1,\mathbf{x}_2\}\\ \mathbf{x}\neq\tilde{\mathbf{x}}}}\left\|\mathbf{H}\left(\mathbf{x}-\tilde{\mathbf{x}}\right)\right\|^2, \tag{11}$$

which is the minimum free distance between all legitimate vectors $\mathbf{x}$ and $\tilde{\mathbf{x}}\in\{\mathbf{x}_1,\mathbf{x}_2\}$.

III. Power Allocation Aided ESDIM Scheme

Based on the proposed ESDIM scheme, we investigate the PA schemes to improve the system reliability.

A. Total Transmit Power Constraint for ESDIM

The TTPC-PA aided scheme for ESDIM can be cast into a transmit precoding problem, in which a PA matrix is calculated to further lower the overall error probability P_{SER}. We introduce the following PA matrix $\mathbf{P}$ expressed as

$$\mathbf{P}=\text{diag}([p_1,p_2,\ldots,p_N]) \tag{12}$$

to precode $\mathbf{x},\tilde{\mathbf{x}}\in\{\mathbf{x}_1,\mathbf{x}_2\}$ along with the total power constraint $\sum_{i=1}^N p_i^2\le P_T$, where p_i is the transmit power of the UE when it steers its main lobe to the i-th candidate RRH. Thus, the received signal at the CBPU is

$$\mathbf{y}=\mathbf{HPx}+\mathbf{n},\ \mathbf{x}\in\left\{\mathbf{x}_1,\mathbf{x}_2\right\}, \tag{13}$$

and the corresponding ML detector is

$$\begin{cases}\left[\hat{i},\hat{n}_0\right]=\arg\min\limits_{i,n_0}\|\mathbf{y}-\mathbf{HPx}\|^2,\\ \left[\hat{a},\hat{b},\hat{n}_1,\hat{n}_2\right]=\arg\min\limits_{a,b,n_1,n_2}\|\mathbf{y}-\mathbf{HPx}\|^2.\end{cases} \tag{14}$$

Therefore, the metric in (11) can be rewritten as

$$d_{\min}(\mathbf{P})=\min_{\substack{\mathbf{x},\tilde{\mathbf{x}}\in\{\mathbf{x}_1,\mathbf{x}_2\}\\ \mathbf{x}\neq\tilde{\mathbf{x}}}}\left\|\mathbf{HP}\left(\mathbf{x}-\tilde{\mathbf{x}}\right)\right\|^2. \tag{15}$$

In order to obtain the PA matrix, we need to solve the problem

$$\begin{cases}\mathbf{P}_{\text{optimal}}=\max\limits_{\mathbf{P}}d_{\min}(\mathbf{P})\\ \text{s.t.}\ \ tr\left(\mathbf{P}^H\mathbf{P}\right)\le P_T\end{cases}, \tag{16}$$

where P_T is the total transmit power.

If $N>2$, it is an open challenge to obtain a closed-form solution for (16). Then, we propose an iterative TTPC-PA algorithm to obtain a suboptimal solution to (16), where only a special BDs pair $(\bar{m},\bar{n})$ associated with the minimum free distance $d_{\min}(\mathbf{P})$ is considered for power allocation. Taking the specific configuration with $N=4$ RRHs as an example, the iterative TTPC-PA algorithm can be summarized as follows:

- Step 1: Initialize $\mathbf{P}=\text{diag}([1,1,1,1])$ and the iteration counter $l=1$;
- Step 2: Calculate all possible error vectors according to
$$\mathbf{e}'_{s,t}=\mathbf{x}_s-\mathbf{x}_t,\quad \mathbf{x}_s,\mathbf{x}_t\in\{\mathbf{x}_1,\mathbf{x}_2\}, \tag{17}$$
and then remove the collinear error vectors with $\mathbf{e}'_{l_s}=g\mathbf{e}'_{l_t}(g\in\{\pm1,\pm i\})$;
- Step 3: Calculate the free distance with PA matrix $\mathbf{P}$ for the error vectors in (17) and find the one that minimizes $d_{\min}(\mathbf{P})$. The corresponding pair is denoted by $(\bar{m},\bar{n})$;
- Step 4: Keep the $\bar{m}$-th and $\bar{n}$-th power coefficients as unknown parameters, and set the others to 1. Then, find the optimal PA matrix $\mathbf{P}_{\text{opt}}^{(\bar{m},\bar{n})}$ according to (16);
- Step 5: Examine $\mathbf{P}_{\text{opt}}^{(\bar{m},\bar{n})}$ and check if $d_{\min}(\mathbf{P}_{\text{opt}}^{(\bar{m},\bar{n})})\ge d_{\min}(\mathbf{P})$. If not, set $l=l+1$, select the pair with the l-th minimum free distance, and then go back to Step 3.

The matrix $\mathbf{P}_{\text{opt}}^{(\bar{m},\bar{n})}$ in Step 4 is obtained as follows. Let us assume that the current selected BD pair is $(\bar{m},\bar{m})=(1,2)$. Then, $p_3=p_4=1$. Let us define the error vector pair $(\mathbf{e}'_{l_1},\mathbf{e}'_{l_2})$ with e^α_β denoting the αth $(1\le\alpha\le4)$ element of $\mathbf{e}'_\beta(\beta=l_1,l_2)$,

$$\begin{cases}\mathbf{e}'_{l_1}=\left[e^1_{l_1},e^2_{l_1},e^3_{l_1},e^4_{l_1}\right]^T,\\ \mathbf{e}'_{l_2}=\left[e^1_{l_2},e^2_{l_2},e^3_{l_2},e^4_{l_2}\right]^T.\end{cases} \tag{18}$$

The corresponding free distances are

$$\begin{aligned}d_{l_1}=\left\|\mathbf{HPe}'_{l_1}\right\|^2&=a_1^{l_1}p_1^2+p_1\left(p_2b_{12}^{l_1}+b_{13}^{l_1}+b_{14}^{l_1}\right)\\&\quad+a_2^{l_1}p_2^2+p_2\left(b_{23}^{l_1}+b_{24}^{l_1}\right)\\&\quad+a_3^{l_1}+b_{34}^{l_1}+a_4^{l_1},\end{aligned} \tag{19}$$

$$\begin{aligned}d_{l_2}=\left\|\mathbf{HPe}'_{l_2}\right\|^2&=a_1^{l_2}p_1^2+p_1\left(p_2b_{12}^{l_2}+b_{13}^{l_2}+b_{14}^{l_2}\right)\\&\quad+a_2^{l_2}p_2^2+p_2\left(b_{23}^{l_2}+b_{24}^{l_2}\right)\\&\quad+a_3^{l_2}+b_{34}^{l_2}+a_4^{l_2},\end{aligned} \tag{20}$$

where

$$\begin{cases}a_j^i=|e_{i,j}|^2\|\mathbf{h}_j\|^2,\\ b_{s,t}^i=2Re\left\{e_{i,s}^*e_{i,t}\mathbf{h}_s^H\mathbf{h}_t\right\},\\ i=l_1,l_2,1\le j\le4,1\le s\le t\le4.\end{cases} \tag{21}$$

Assume $d_{l_1}=d_{l_2}$ and the total power constraint $p_1^2+p_2^2=P_T-2$. The power coefficients can be obtained by solving the

following system of equations

$$\begin{cases} Ap_1^2 + p_1\left[Bp_2 + C\right] + Dp_2^2 + Ep_2 + F = 0 \\ p_1^2 + p_2^2 = P_T - 2 \end{cases} \tag{22}$$

where

$$\begin{cases} A = a_1^{l_1} - a_1^{l_2}, B = b_{12}^{l_1} - b_{12}^{l_2}, \\ C = b_{13}^{l_1} - b_{13}^{l_2} + b_{14}^{l_1} - b_{14}^{l_2}, \\ D = a_2^{l_1} - a_2^{l_2}, \\ E = b_{23}^{l_1} - b_{23}^{l_2} + b_{24}^{l_1} - b_{24}^{l_2}, \\ F = a_3^{l_1} + b_{34}^{l_1} + a_4^{l_1} - a_3^{l_2} - b_{34}^{l_2} - a_4^{l_2}. \end{cases} \tag{23}$$

The system of equations in (22) can be solved in the following cases:

- Case 1: When $A = a_1^{l_1} - a_1^{l_2} \neq 0$, (22) is a quadratic function of p_1. If the discriminant

$$\begin{aligned} \Delta &= \sqrt{\left[Bp_2 + C\right]^2 - 4A\left(Dp_2^2 + Ep_2 + F\right)} \\ &= \sqrt{\left(B^2 - 4AD\right)p_2^2 + \left(2B - 4AE\right)p_2 + C^2 - 4AF} \end{aligned} \tag{24}$$

  can be factorized in the form $\Delta = \sqrt{\left(B'p_2 + C'\right)^2}$ with

$$\begin{cases} B'^2 = B^2 - 4AD \\ 2B'C' = 2B - 4AE \\ C'^2 = C^2 - 4AF \end{cases} \tag{25}$$

  then, we obtain a linear relationship for p_1 and p_2

$$p_1 = \frac{\left(B' - B\right)}{2\,A}p_2 + \frac{\left(C' - C\right)}{2\,A}. \tag{26}$$

  Accounting for the total power constraint $p_1^2 + p_2^2 = P_T - 2$

$$\begin{cases} p_1 = \frac{\left(B' - B\right)}{2\,A}p_2 + \frac{\left(C' - C\right)}{2\,A} \\ p_1^2 + p_2^2 = P_T - 2 \end{cases}, \tag{27}$$

  the power coefficients p_1 and p_2 are equal to

$$\begin{cases} p_1 = \frac{-2MN + \sqrt{4M^2N^2 - 4\left(M^2+1\right)\left(N^2+2-P_T\right)}}{2\left(M^2+1\right)}M + N, \\ p_2 = \frac{-2MN + \sqrt{4M^2N^2 - 4\left(M^2+1\right)\left(N^2+2-P_T\right)}}{2\left(M^2+1\right)}, \end{cases} \tag{28}$$

  where $M = \frac{\left(B' - B\right)}{2\,A}$ and $N = \frac{\left(C' - C\right)}{2\,A}$.
- Case 2: If (24) cannot be factorized, (22) can be rewritten as a function of $f(p_1, p_2)$ and $g(p_1, p_2)$ defined as

$$\begin{cases} f\left(p_1, p_2\right) = a_0\left(p_2\right)p_1^2 + a_1\left(p_2\right)p_1 + a_2\left(p_2\right) \\ g\left(p_1, p_2\right) = b_0\left(p_2\right)p_1^2 + b_1\left(p_2\right)p_1 + b_2\left(p_2\right) \end{cases}. \tag{29}$$

  Let us set $f(p_1, p_2) = 0$ and $g(p_1, p_2) = 0$

$$\begin{cases} f\left(p_1, p_2\right) = 0 \\ g\left(p_1, p_2\right) = 0 \end{cases}. \tag{30}$$

  From (30), the determinant is

$$R_{p_1}(f, g) = \begin{vmatrix} a_0\left(p_2\right) & a_1\left(p_2\right) & a_2\left(p_2\right) & 0 \\ 0 & a_0\left(p_2\right) & a_1\left(p_2\right) & a_2\left(p_2\right) \\ b_0\left(p_2\right) & b_1\left(p_2\right) & b_2\left(p_2\right) & 0 \\ 0 & b_0\left(p_2\right) & b_1\left(p_2\right) & b_2\left(p_2\right) \end{vmatrix}, \tag{31}$$

  where

$$\begin{cases} a_0\left(p_2\right) = A, a_1\left(p_2\right) = Bp_2 + C, \\ a_2\left(p_2\right) = Dp_2^2 + Ep_2 + F, \\ b_0\left(p_2\right) = 1, b_1\left(p_2\right) = 0, \\ b_2\left(p_2\right) = p_2^2 + 2 - P_T. \end{cases} \tag{32}$$

  We can then expand $R_{p_1}(f, g)$ with respect to the 1-st column as $R_{p_1}(f, g) =$

$$\begin{aligned} &A\begin{vmatrix} A & Bp_2 + C & Dp_2^2 + Ep_2 + F \\ 0 & p_2^2 + 2 - P_T & 0 \\ 1 & 0 & p_2^2 + 2 - P_T \end{vmatrix} \\ &+\begin{vmatrix} Bp_2 + C & Dp_2^2 + Ep_2 + F & 0 \\ A & Bp_2 + C & Dp_2^2 + Ep_2 + F \\ 1 & 0 & p_2^2 + 2 - P_T \end{vmatrix}. \end{aligned} \tag{33}$$

  The 1-st term of (33) can be further expanded with respect to the 2-nd row as

$$A\left(p_2^2 + 2 - P_T\right)\begin{vmatrix} A & Dp_2^2 + Ep_2 + F \\ 1 & p_2^2 + 2 - P_T \end{vmatrix}. \tag{34}$$

  Also, the 2-nd term of (33) can be transformed into

$$\begin{vmatrix} Bp_2 + C & Dp_2^2 + Ep_2 + F & \begin{bmatrix} -\left(Bp_2 + C\right) \times \\ \left(p_2^2 + 2 - P\right) \end{bmatrix} \\ A & Bp_2 + C & \begin{bmatrix} Dp_2^2 + Ep_2 + F \\ -A\left(p_2^2 + 2 - P_T\right) \end{bmatrix} \\ 1 & 0 & 0 \end{vmatrix}, \tag{35}$$

  and can be further expanded with respect to the 3-rd row as

$$\begin{vmatrix} Dp_2^2 + Ep_2 + F & \begin{bmatrix} -\left(Bp_2 + C\right) \times \\ \left(p_2^2 + 2 - P_T\right) \end{bmatrix} \\ Bp_2 + C & \begin{bmatrix} Dp_2^2 + Ep_2 + F \\ -A\left(p_2^2 + 2 - P_T\right) \end{bmatrix} \end{vmatrix}. \tag{36}$$

  Thus, $R_{p_1}(f, g)$ can be formulated as

$$\begin{aligned} R_{p_1}(f, g) &= A^2\left(p_2^2 + 2 - P_T\right)^2 \\ &\quad - 2A\left(p_2^2 + 2 - P_T\right)\left(Dp_2^2 + Ep_2 + F\right) \\ &\quad + \left(Dp_2^2 + Ep_2 + F\right)^2 \\ &\quad + \left(Bp_2 + C\right)\left(p_2^2 + 2 - P_T\right) \\ &= \left[A\left(p_2^2 + 2 - P_T\right) - \left(Dp_2^2 + Ep_2 + F\right)\right]^2 \\ &\quad + \left(Bp_2 + C\right)\left(p_2^2 + 2 - P_T\right) \\ &= \left[\left(A - D\right)p_2^2 - Ep_2 + 2\,A - AP_T - F\right]^2 \\ &\quad + \left(Bp_2 + C\right)\left(p_2^2 + 2 - P_T\right). \end{aligned} \tag{37}$$

  From (37), the equation $R_{p_1}(f, g) = 0$ has solutions only when

$$\begin{cases} \left(A - D\right)p_2^2 - Ep_2 + 2\,A - AP_T - F = 0 \\ Bp_2 + C = 0 \end{cases}, \tag{38}$$

since $p_2^2+2-P_T<0$ for any valid p_2 satisfying the total power constraint $p_1^2+p_2^2=P_T-2$. Furthermore, the following special cases are in order:
i) When $A-D\neq 0$ and $B=C=0$, we obtain

$$p_2=\frac{\sqrt{E^2-4\left(A-D\right)\left(2\,A-AP_T-F\right)}}{2\left(A-D\right)}+\frac{E}{2\left(A-D\right)}, \tag{39}$$

and thus $p_1=\sqrt{P_T-2-p_1^2}$.
ii) When $B\neq 0$, we need to examine if $p_2=-\frac{C}{B}$ is a solution for (38). If it is the case, we obtain

$$\begin{cases} p_1=\sqrt{P_T-2-\frac{C^2}{B^2}}, \\ p_2=-\frac{C}{B}, \end{cases} \tag{40}$$

- Case 3: When $A=a_1^{l_1}-a_1^{l_2}=0$, and $D=a_2^{l_1}-a_2^{l_2}=0$, (22) reduces to

$$\begin{cases} p_1\left[Bp_2+C\right]+Ep_2+F=0 \\ p_1^2+p_2^2=P_T-2 \end{cases}. \tag{41}$$

By using similar steps as those used for Case 2, the corresponding $R_{p_1}(f,g)$ is expressed as

$$R_{p_1}(f,g)=\begin{vmatrix} 0 & Bp_2+C & Ep_2+F & 0 \\ 0 & 0 & Bp_2+C & Ep_2+F \\ 1 & 0 & p_2^2+2-P_T & 0 \\ 0 & 1 & 0 & p_2^2+2-P_T \end{vmatrix}. \tag{42}$$

Equation (42) can be expanded with respect to the 1-st column as

$$\begin{aligned} R_{p_1}(f,g) &= \begin{vmatrix} Bp_2+C & Ep_2+F & 0 \\ 0 & Bp_2+C & Ep_2+F \\ 1 & 0 & p_2^2+2-P_T \end{vmatrix} \\ &= \left(Bp_2+C\right)^2\left(p_2^2+2-P_T\right)+\left(Ep_2+F\right)^2. \end{aligned} \tag{43}$$

Similar to (37), only when $Bp_2+C=0$ and $Ep_2+F=0$ a solution for $R_{p_1}(f,g)=0$ exists. Thus, the condition $\frac{F}{E}=\frac{C}{B}$ needs to be fulfilled. Accordingly, the power coefficients are

$$\begin{cases} p_1=\sqrt{P_T-2-\frac{F^2}{E^2}}, \\ p_2=-\frac{F}{E}. \end{cases} \tag{44}$$

Thus, we can obtain a candidate PA matrix $\mathbf{P}_{l_1,l_2}$ corresponding to the error vector pair $(\mathbf{e}'_{l_1},\mathbf{e}'_{l_2})$. Next, we calculate the PA matrices for other error vector pairs $(\mathbf{e}'_{l_1},\mathbf{e}'_{l_2})(\mathbf{e}'_{l_1},\mathbf{e}'_{l_2}\in\mathbb{E},\mathbf{e}'_{l_1}\neq\mathbf{e}'_{l_2})$ and denote the set of all candidate PA matrices by $\mathbb{P}$ and the set of nonlinear error vectors by $\mathbb{E}$. Then, we calculate the free distance $d_l(l=1,2,3,\ldots)$ for all nonlinear error vectors $\mathbf{e}_l$ with respect to every $\mathbf{P}_{\text{candi}}$. The optimal PA matrix $\mathbf{P}_{\text{opt}}^{(\bar{m}=1,\bar{n}=1)}$ is defined as

$$\mathbf{P}_{\text{opt}}^{(\bar{m}=1,\bar{n}=2)}=\arg\max_{\mathbf{P}\in\mathbb{P}}\left\{\min\left\{d_1,d_2,\ldots,d_{|\mathbb{E}|}\right\}\right\}. \tag{45}$$

Then $\mathbf{P}_{\text{opt}}^{(\bar{m}=1,\bar{n}=2)}$ is examined according to Step 5.

B. Average Per-Beamformer Power Constraint for ESDIM

In this section, we investigate the APBPC-PA aided scheme for the ESDIM system as a more practical extension of the TTPC-PA aided scheme. Specifically, the following additional power constraint is applied to the average power of each beamformer when transmitting information symbols

$$\begin{cases} (a)\ E\left\{\left|p_ix_i\right|^2\right\}\leq\frac{P_T}{N},1\leq i\leq N \\ (b)\ \begin{cases} E\left\{\left|p_ax_a\right|^2\right\}\leq\frac{P_T}{N} \\ E\left\{\left|p_bx_b\right|^2\right\}\leq\frac{P_T}{N} \end{cases},1\leq a,b\leq N \end{cases}, \tag{46}$$

where (a) in (46) is for the case of only one activated BD, and (b) in (46) is for the case of two activated BDs. Also, x_i, x_a and x_b are the i-th, a-th and b-th element of $\mathbf{x}\in\{\mathbf{x}_1,\mathbf{x}_2\}$, respectively. The additional power constraint in (46) imposes an upper limit on the average power of the transmitted symbol and it stems from the practical implementation of the proposed system [42], [43], [44], [45], [46], where the power amplifiers may be deployed at the transmitter side.

Similar to the TTPC-PA adied scheme, we consider the APBPC-PA aided scheme for a given selected beamforming pair $(\bar{m},\bar{n})$, while the other two power coefficients are set to 1. The APBPC-PA matrices can be computed similar to the iterative TTPC-PA method

$$\begin{cases} \mathbf{P}_{\text{APBPC}}=\max_{\mathbf{P}}d_{\min}(\mathbf{P}) \\ tr\left(\mathbf{P}^H\mathbf{P}\right)\leq P_T \\ \begin{cases} (a)\ E\left\{\left|p_ix_i\right|^2\right\}\leq\frac{P_T}{N},1\leq i\leq N \\ (b)\ \begin{cases} E\left\{\left|p_ax_a\right|^2\right\}\leq\frac{P_T}{N} \\ E\left\{\left|p_bx_b\right|^2\right\}\leq\frac{P_T}{N} \end{cases},1\leq a,b\leq N \end{cases} \end{cases}. \tag{47}$$

Based on Step 5 and according to [45], the conditions to be evaluated are

$$\begin{cases} d_{\min}(\mathbf{P}_{\text{opt}}^{(\bar{m},\bar{n})})\geq d_{\min}(\mathbf{P}) \\ E\left\{\left|p_ix_i\right|^2\right\}\leq\frac{P_T}{N},1\leq i\leq N \\ \begin{cases} E\left\{\left|p_ax_a\right|^2\right\}\leq\frac{P_T}{N} \\ E\left\{\left|p_bx_b\right|^2\right\}\leq\frac{P_T}{N} \end{cases},1\leq a,b\leq N \end{cases}, \tag{48}$$

where the candidate PA matrix $\mathbf{P}_{\text{opt}}^{(\bar{m},\bar{n})}$ is to be examined with respect to $\mathbf{x}\in\{\mathbf{x}_1,\mathbf{x}_2\}$. More specifically, we need first to extract all matrices $\mathbf{P}^{(\bar{m},\bar{n})}\in\mathbb{P}$ that meet the condition $d_{\min}(\mathbf{P}^{(\bar{m},\bar{n})})\geq d_{\min}(\mathbf{P})$. The obtained matrices $\mathbf{P}^{(\bar{m},\bar{n})}$ constitute a subset $\mathbb{E}_0$ based on the following order

$$d_{\min}(\mathbf{P}_1^{(\bar{m},\bar{n})})\geq d_{\min}(\mathbf{P}_2^{(\bar{m},\bar{n})})\geq\ldots\geq d_{\min}(\mathbf{P}_{|\mathbb{E}_0|}^{(\bar{m},\bar{n})}). \tag{49}$$

Based on (49), the matrix $\mathbf{P}_k^{(\bar{m},\bar{n})}$ that fulfills the conditions in (46) is selected as the final APBPC PA matrix $\mathbf{P}_{\text{APBPC}}$.

C. Strict Per-Beamformer Power Constraint for ESDIM

In this section, we consider an even stricter power constraint for each beamformer as

$$\begin{cases} (a)\ \max\left\{|p_i x_i|^2\right\} \le \frac{P_T}{N}, 1 \le i \le N \\ (b)\ \begin{cases} \max\left\{|p_a x_a|^2\right\} \le \frac{P_T}{N} \\ \max\left\{|p_b x_b|^2\right\} \le \frac{P_T}{N} \end{cases}, 1 \le a, b \le N \end{cases}, \tag{50}$$

The constraints (a) and (b) in (50) refer to the case of only one activated BD and two activated BDs, respectively. Similar to the APBPC-PA aided scheme, we have the following

$$\begin{cases} \mathbf{P}_{\text{SPBPC}} = \max\limits_{\mathbf{P}} d_{\min}(\mathbf{P}) \\ tr\left(\mathbf{P}^H\mathbf{P}\right) \le P_T \\ \begin{cases} (a)\ \max\left\{|p_i x_i|^2\right\} \le \frac{P_T}{N}, 1 \le i \le N \\ (b)\ \begin{cases} \max\left\{|p_a x_a|^2\right\} \le \frac{P_T}{N} \\ \max\left\{|p_b x_b|^2\right\} \le \frac{P_T}{N} \end{cases}, 1 \le a, b \le N \end{cases} \end{cases}. \tag{51}$$

Thus, the conditions to be analyzed in Step 5 are

$$\begin{cases} d_{\min}(\mathbf{P}_{\text{opt}}^{(\bar{m},\bar{n})}) \ge d_{\min}(\mathbf{P}) \\ \max\left\{|p_i x_i|^2\right\} \le \frac{P_T}{N}, 1 \le i \le N \\ \begin{cases} \max\left\{|p_a x_a|^2\right\} \le \frac{P_T}{N} \\ \max\left\{|p_b x_b|^2\right\} \le \frac{P_T}{N} \end{cases}, 1 \le a, b \le N \end{cases}. \tag{52}$$

Let $s_{\max}^1, s_{\max}^2$ denote the primary signal symbol and secondary signal symbol with the largest magnitude

$$\begin{aligned} s_{\max}^1 &= \arg\max_{s\in\mathbb{S}_1} |s|, \\ s_{\max}^2 &= \arg\max_{s\in\mathbb{S}_2} |s|, \end{aligned} \tag{53}$$

respectively. The power constraint can then be rewritten as

$$\begin{cases} (a)\ \ |p_i x_i|^2 \le \frac{P_T}{N|s_{\max}^1|^2}, 1 \le i \le N \\ (b)\ \ \begin{cases} |p_a x_a|^2 \le \frac{P_T}{N|s_{\max}^2|^2} \\ |p_b x_b|^2 \le \frac{P_T}{N|s_{\max}^2|^2} \end{cases}, 1 \le a, b \le N \end{cases}. \tag{54}$$

The PA matrix $\mathbf{P}_{\text{SPBPC}}$ can then be obtained similarly to the APBPC-PA aided scheme, but considering the new stricter constraint.

IV. Simulation Results

In this section, we first compare the SER of the proposed ESDIM scheme, the SDIM scheme in [32] that exploits only one BD, and the generalized SDIM (GSDIM) scheme in [33] that exploits a fixed number of BDs. Then we investigate the influence of the UE beamforming side lobe gain parameter m on the SER. In addition, the SER of the three proposed PA-aided schemes, i.e. the TTPC PA-aided scheme, the APBPC-aided scheme and the SPBPC-aided scheme, are extensively evaluated. Moreover, the impact of imperfections on the channel side information on the TTPA PA-aided scheme are investigated. The simulation parameters are summarized in Table I. Specifically, we assume that $N = 2, 4$ candidate RRHs are selected from $N_0 = 3, 6$ possible ones, and the distances of the UE to these candidate RRHs are

$$\begin{cases} \mathbf{d}_1 = [d_1, 1.2d_1, 1.9d_1, 3d_1, 4.5d_1, 5.2d_1], \\ \mathbf{d}_2 = [d_1, 1.5d_1, 2.7d_1, 3.5d_1, 4d_1, 4.8d_1], \end{cases}$$

for $(N, N_0) = (4, 6)$, and

$$\begin{cases} \mathbf{d}_3 = [d_1, 1.3d_1, 1.5d_1], \\ \mathbf{d}_4 = [d_1, 1.7d_1, 2.3d_1], \end{cases}$$

for $(N, N_0) = (2, 3)$, where d_1 represents the shortest distance of the UE to the RRHs in each configuration. Besides, two transmission rates are considered, i.e., $R_b = 6$ and 8 bits/symbol for $N = 4$, where the corresponding primary modulations are QPSK, 16QAM for the proposed ESDIM, QPSK and 8PSK for the GSDIM with two fixed BDs, and 16QAM and 64QAM for the SDIM with single-beamforming-direction (SBD). As for the rate of 4 bits/symbol and 6 bits/symbol for $N = 2$, the modulation schemes for SDIM are 8PSK and 32QAM, respectively.

TABLE I
Main Simulation Parameters

Parameters	Specifications	Values
N_t	Number of UE antennas	16
N_r	Number of RRH antennas	128
N_0	Number of available RRHs	3, 6
N	Number of candidate RRHs	2, 4
N_s	Modulation order of ESDIM	QPSK, 16QAM
M	Main lobe gain of UE beam (dB)	10
m	Side lobe gain of UE beam (dB)	-10
G	Side lobe gain of RRH beam (dB)	10
β	Path loss factor	2.5
d_1	Shortest distance of UE&RRH (m)	300

Fig. 3 compares the SER of the proposed ESDIM, GSDIM in [33] and SBD-SDIM schemes in [33], where the transmission rates are $R_b = 4$ bits/symbol and $R_b = 6$ bits/symbol. As for the the GSDIM scheme with $N = 4$ candidate RRHs, selecting 2 out of 4 candidate RRHs results in 6 combinations. With $\mathcal{C}_N^2 = 6$ and $\log_2 6 = 2.585$, an integer number of bits cannot represent all the combinations, and thus we ignore the two combinations with the most severe path loss and only consider four combinations. As can be observed from Fig. 3, for $(N, N_0) = (4, 6)$ with

$$\begin{cases} \mathbf{d}_1^* = [d_1, 1.2d_1, 1.9d_1, 3d_1], \\ \mathbf{d}_2^* = [d_1, 1.5d_1, 2.7d_1, 3.5d_1], \end{cases}$$

the proposed ESDIM scheme provides an SNR gain of 2 dB, compared with the SDIM scheme at the SER of 10^{-5} under $\mathbf{d}_1$, and about 1 dB with respect to the GSDIM scheme. At the SER of 10^{-3}, the proposed scheme still achieves a better SNR

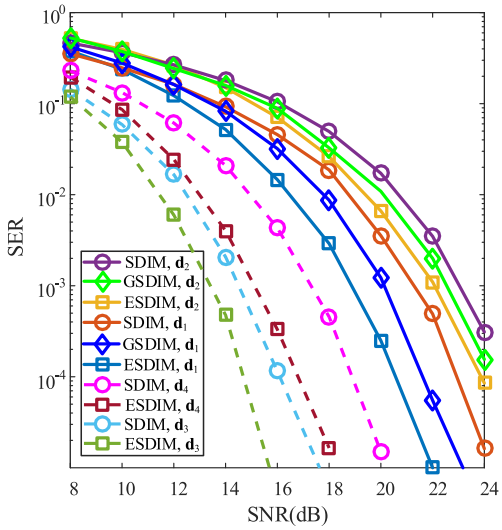

Fig. 3. SER comparison of the proposed ESDIM, GSDIM in [33] and SBD-SDIM in [32], for the transmission rates of 4, 6 bits/symbol and distance vectors $\mathbf{d}_1$, $\mathbf{d}_2$, $\mathbf{d}_3$, and $\mathbf{d}_4$. The solid and dashed lines represent the results for $N = 4$ and $N = 2$, respectively.

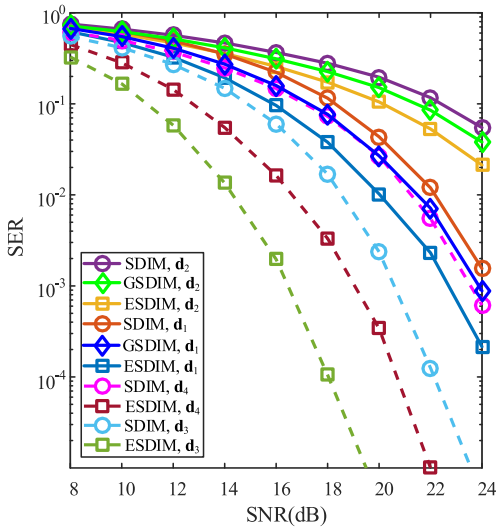

Fig. 4. SER comparison of the proposed ESDIM, GSDIM in [33] and SBD-SDIM in [32], for the transmission rates of 6, 8 bits/symbol and distance vectors $\mathbf{d}_1$, $\mathbf{d}_2$, $\mathbf{d}_3$, and $\mathbf{d}_4$. The solid and dashed lines represent the results for $N = 4$ and $N = 2$, respectively.

outperforming of about 1 dB and 0.5 dB the GSDIM and SDIM schemes, respectively, under $\mathbf{d}_2$. When $(N, N_0) = (2, 3)$, i.e., only two candidate RRHs, with

$$\begin{cases} \mathbf{d}_3^* = [d_1, 1.3d_1], \\ \mathbf{d}_4^* = [d_1, 1.7d_1], \end{cases}$$

QPSK and 8QAM are employed for the ESDIM and SBD-SDIM schemes. As can be seen from the two sets of results (dashed lines) in Fig. 3, the proposed ESDIM scheme achieves a better SER and the SNR gain is about 2 dB at a SER of 10^{-5}.

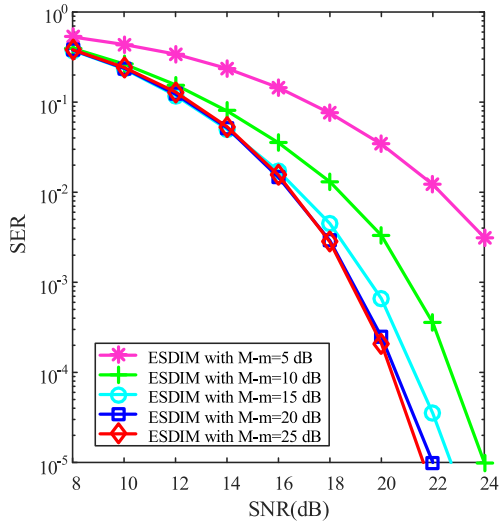

Fig. 5. Impact of the side lobe gain of the UE on the SER performance of the ESDIM system, where the QPSK modulation is employed, under the transmission of 6 bits/symbol and distance vector $\mathbf{d}_1 = [d_1, 1.2d_1, 1.9d_1, 3d_1, 4.5d_1, 5.2d_1]$.

Results for higher order APM modulation are shown in Fig. 4. As can be seen from the figure, for $(N, N_0) = (4, 6)$, the proposed scheme achieves an SNR gain of about 1.8 dB and 1.5 dB at the SER of 10^{-3} with $\mathbf{d}_1^*$. It is also observed that the SER for a higher transmission rate deteriorates much faster compared to Fig. 3, especially for $\mathbf{d}_2^*$. This is attributed mainly to the combined effect of higher order modulation. The SER gains stem from encoding data onto the combination of the number of activated BDs and the primary-secondary constellation structure, which enables the proposed scheme to employ a lower order APM modulation than the SDIM scheme with the same transmit rate. In addition, from the perspective of reliability, there is always a probability of a better connection (e.g., a shorter distance) between the UE and RRH in the available transmit mode of two-beamforming-direction mode, and this better connection helps reduce the overall error rate. In the SDIM scheme, only one BD is activated, and the overall system reliability is hindered by the single activated BD. Besides, when there are only $N = 2$ candidate RRHs, the superiority of the proposed scheme is more obvious and it is about 4 dB at the SER of 10^{-5} under $\mathbf{d}_3$. In addition, the proposed scheme is capable of achieving larger SNR gains when the path loss is more severe (i.e., under distance vector $\mathbf{d}_4$).

In Fig. 5, we investigate the influence of the beamforming side lobe gain of the UE. The main lobe gain of the UE is fixed to 10 dB. As can be seen from Fig. 5, as the side lobe gain m decreases, the SER performance becomes better. This is because, in each transmission, the UE steers its beam main lobes towards the RRHs. A smaller m means that more transmit power is concentrated on the main lobes and there is less transmit power allocated to the side lobes.

Fig. 6 compares the SER of the PA-aided schemes and equal-gain (EG) schemes of the proposed ESDIM system with varying orders for APM modulation and different numbers of candidate

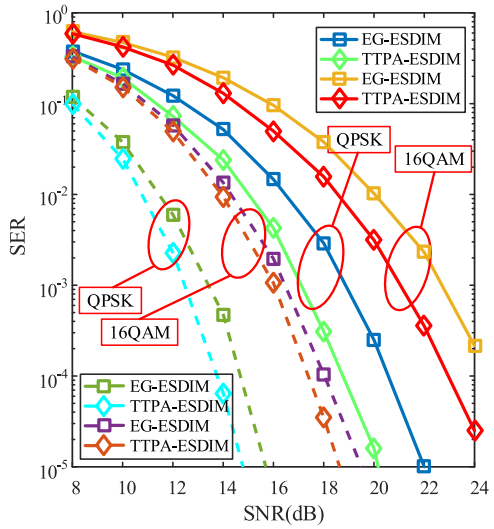

Fig. 6. SER comparison of the proposed TTPC-aided and the equal-gain (EG) ESDIM, where the QPSK and 16QAM modulations are employed, respectively, with distance vector $\mathbf{d}_1$ and $\mathbf{d}_3$ for $N = 4, 2$. The solid lines represent the results of $N = 4$, dashed lines represent the results of $N = 2$.

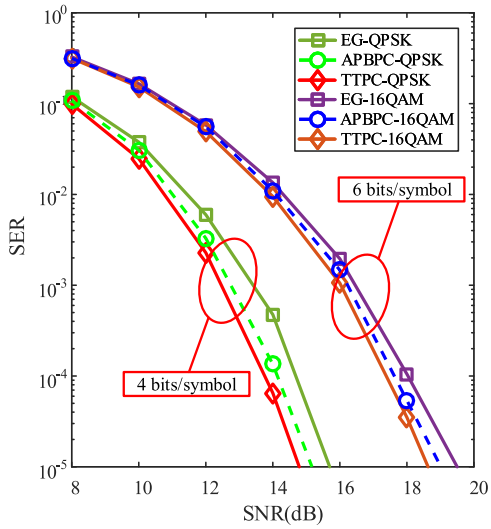

Fig. 8. SER comparison of the TTPC-PA aided, APBPC-PA aided and EG ESDIM schemes with $N = 2$, for the transmission rates of 4 bits/symbol and 6 bits/symbol with distance vector $\mathbf{d}_3$, where the QPSK and 16QAM modulation schemes are employed, respectively.

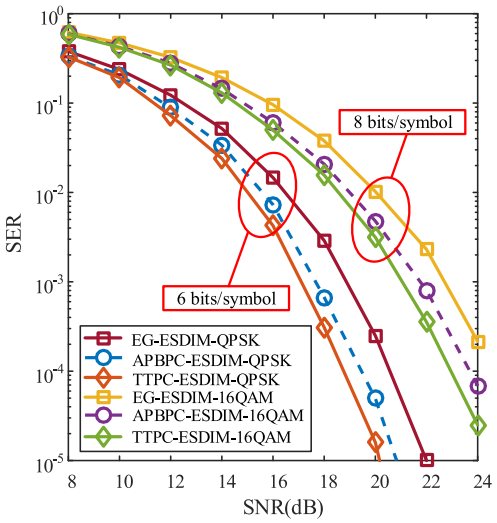

Fig. 7. SER comparison of the TTPC-PA aided, APBPC-PA aided and EG ESDIM schemes with $N = 4$, for the transmission rates of 6 bits/symbol and 8 bits/symbol with distance vector $\mathbf{d}_1$, where the QPSK and 16QAM modulation schemes are employed, respectively.

RRHs. The transmission rates of the schemes with $N = 4$ candidate RRHs using QPSK and 16QAM are 6 bits/symbol and 8 bits/symbol, and for the schemes with $N = 2$ candidate RRHs, the transmission rates are 4 bits/symbol and 6 bits/symbol, respectively. In general, the PA-aided schemes (TTPA-ESDIM) can achieve SNR gains over the EG schemes (EG-ESDIM).

Figs. 7 and 8 show the SER of the TTPC-PA aided, the APBPC-PA aided and the EG ESDIM schemes. It can be seen from Figs. 7 and 8 that the TTPC-PA aided and APBPC-PA aided schemes can provide considerable SNR gains over the EG scheme, for the transmission rates of 4 bits/symbol, 6 bits/symbol and 8 bits/symbol. Specifically, as can be seen from Fig. 7, at the transmission rate of 6 bits/symbol, the TTPC-PA aided ESDIM scheme is capable of achieving an SNR gain of 2 dB over the EG ESDIM scheme at the SER of 10^{-5}. As for the case study with 16QAM, the TTPC-PA aided scheme provides an SNR gain of about 2 dB at the SER of 10^{-3}. As for the APBPC-PA aided scheme, Fig. 7 shows that it can achieve an SNR gain of about 1.2 dB over the EG ESDIM scheme at SER $= 10^{-5}$, and that the gain is about 0.8 dB under the transmission rate of 8 bits/symbol at the SER of 10^{-3}. It can also be observed from Fig. 7 that the SER of the APBPC-PA aided scheme is inferior to that of the TTPC-PA aided scheme. The gap is about 0.8 dB at SER $= 10^{-5}$ for the transmission rate of 6 bits/symbol. The reason is that the power coefficients calculated using APBPC-PA are restricted in a smaller range. In addition, as shown in Fig. 8, when the transmission rates are 4 bits/symbols and 6 bits/symbol (for $N = 2$), the proposed TTPC-aided and APBPC-aided schemes can still provide SNR gains. At the SER of 10^{-5}, the SNR gains are about 1 dB for the TTPC-aided schemes and 0.6 dB for the APBPC-aided schemes.

Moreover, Figs. 9 and 10 show the SER of the SPBPC-PA aided ESDIM scheme, the TTPC-PA aided scheme and the EG schemes for the transmission rates of 4 bits/symbol, 6 bits/symbol and 8 bits/symbol. As shown in Fig. 9, the SPBPC-PA aided ESDIM scheme outperforms its EG counterpart by about 0.8 dB at SER $= 10^{-5}$ for the transmission rate of 6 bits/symbol. At a SER of 10^{-3}, the gain is about 0.6 dB for the transmission rate of 8 bits/symbol. At the rate of 8 bits/symbol, the SPBPC-PA aided scheme also achieves some SNR gains. For the case of $N = 2$ candidate RRHs, the SNR gain of the SPBPC-PA aided scheme is about 0.5 dB. In addition, compared with the simulation results in Figs. 7–10, the SNR gains of the SPBPC-PA aided scheme are not as good as that of the TTPC-PA aided ESDIM scheme. Under the considered transmission rates and different numbers of candidate RRHs, the SER curves of the

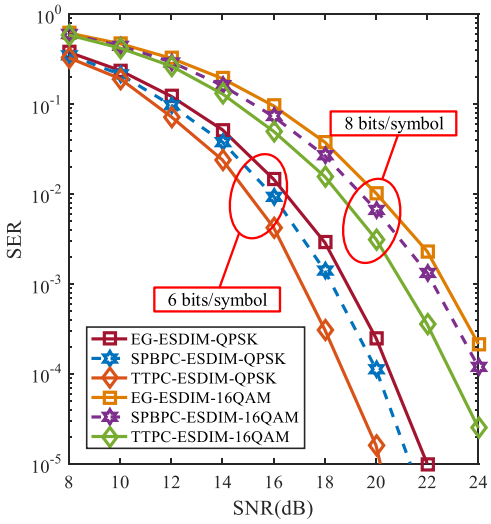

Fig. 9. SER comparison of the TTPC-PA aided, SPBPC-PA aided and EG ESDIM schemes with $N = 4$, for the transmission rates of 6 bits/symbol and 8 bits/symbol with distance vector $\mathbf{d}_1$, where the QPSK and 16QAM modulation schemes are employed, respectively.

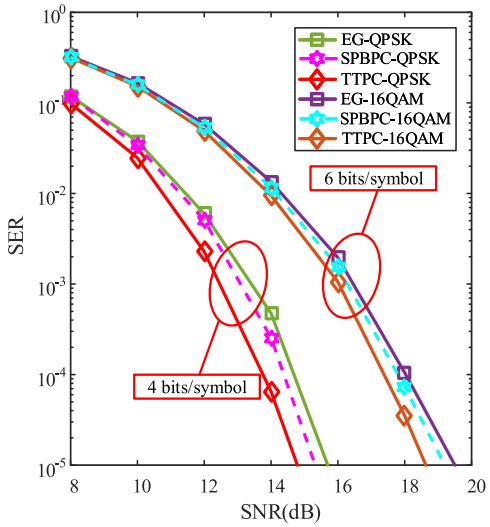

Fig. 10. SER comparison of the TTPC-PA aided, SPBPC-PA aided and EG ESDIM schemes with $N = 2$, for the transmission rates of 4 bits/symbol and 6 bits/symbol with distance vector $\mathbf{d}_3$, where the QPSK and 16QAM modulation schemes are employed, respectively.

SPBPC-PA aided scheme are closer to those of the EG schemes, while the SER curves of the APBPC-PA aided scheme are closer to those of the TTPC-PA aided schemes.

In addition to the SER, as reported in Table II, we compare the spectral efficiency of the proposed ESDIM, GSDIM and SDIM schemes. Generally, due to the larger number of combinations generated from the joint use of multiple constellations and beam directions, the ESDIM schemes can achieve the largest transmission rates.

Based on the results in Figs. 5–9, we can select the appropriate PA strategies based on the desired communication requirements.

TABLE II
SPECTRAL EFFICIENCY OF ESDIM, GSDIM AND SDIM

Number of candidate RRHs	APM	ESDIM (bits/symbol)	GSDIM (bits/symbol)	SDIM (bits/symbol)
2	BPSK	4	2	2
2	QPSK	6	4	3
2	8PSK	8	6	4
4	BPSK	6	4	3
4	QPSK	8	6	4
4	8PSK	10	8	5

V. CONCLUSION

In this paper, we proposed a novel transmission scheme for SDIM-based mmWave communication systems with distributed antennas, in which the combinations of BDs and signal constellations are jointly exploited to transmit information bits. We also improved the reliability of the proposed ESDIM system by means of power allocation, by analyzing three transmit power constraints, i.e., the total transmit power constraint, the average per-beamformer power constraint and the strict per-beamformer power constraint. Simulation results were presented to demonstrate that the proposed scheme is capable of achieving better SER performance under various system configurations, and that the proposed PA approaches can further improve the system reliability.

REFERENCES

[1] T. S. Rappaport et al., "Wireless communications and applications above 100 GHz: Opportunities and challenges for 6G and beyond," *IEEE Access*, vol. 7, pp. 78729–78757, 2019.

[2] P. Yang, Y. Xiao, M. Xiao, and S. Li, "6G wireless communications: Vision and potential techniques," *IEEE Netw.*, vol. 33, no. 4, pp. 70–75, Jul./Aug. 2019.

[3] M. Xiao et al., "Millimeter wave communications for future mobile networks," *IEEE J. Sel. Areas Commun.*, vol. 35, no. 9, pp. 1909–1935, Sep. 2017.

[4] P. Liu and A. Springer, "Space shift keying for LOS communication at mmWave frequencies," *IEEE Wireless Commun. Lett.*, vol. 4, no. 2, pp. 121–124, Apr. 2015.

[5] I. A. Hemadeh, M. El-Hajjar, S. Won, and L. Hanzo, "Multiuser steered multiset space-time shift keying for millimeter-wave communications," *IEEE Trans Veh. Technol.*, vol. 66, no. 6, pp. 5491–5495, Jun. 2017.

[6] C. Sacchi, T. F. Rahman, I. A. Hemadeh, and M. El-Hajjar, "Millimeter-wave transmission for small-cell backhaul in dense urban environment: A solution based on MIMO-OFDM and space-time shift keying (STSK)," *IEEE Access*, vol. 5, pp. 4000–4017, 2017.

[7] I. A. Hemadeh, M. El-Hajjar, S. Won, and L. Hanzo, "Multi-set space-time shift keying and space-frequency space-time shift keying for millimeter-wave communications," *IEEE Access*, vol. 5, pp. 8324–8342, 2016.

[8] I. A. Hemadeh, P. Botsinis, M. El-Hajjar, S. Won, and L. Hanzo, "Reduced-RF-chain aided soft-decision multi-set steered space-time shift-keying for millimeter-wave communications," *IEEE Access*, vol. 5, pp. 7223–7243, 2017.

[9] Y. Ding, K. J. Kim, T. Koike-Akino, M. Pajovic, P. Wang, and P. Orlik, "Millimeter wave adaptive transmission using spatial scattering modulation," in *Proc. IEEE Int. Conf. Commun.*, 2017, pp. 1–6.

[10] Y. Ding, K. J. Kim, T. Koike-Akino, M. Pajovic, P. Wang, and P. Orlik, "Spatial scattering modulation for uplink millimeter-wave systems," *IEEE Commun. Lett.*, vol. 21, no. 7, pp. 1493–1496, Jul. 2017.

[11] X. Zhu, L. Yuan, K. J. Kim, Q. Li, and J. Zhang, "Reconfigurable intelligent surface-assisted spatial scattering modulation," *IEEE Commun. Lett.*, vol. 26, no. 1, pp. 192–196, Jan. 2022.

[12] J. Zhang, Q. Li, L. Yang, K. J. Kim, P. Yang, and S. Ruan, "Adaptive spatial scattering modulation," *IEEE Trans. Wireless Commun.*, vol. 20, no. 10, pp. 6680–6690, Oct. 2021.

[13] M. Lee and W. Chung, "Adaptive multimode hybrid precoding for single-RF virtual space modulation with analog phase shift network in MIMO systems," *IEEE Trans. Wireless Commun.*, vol. 16, no. 4, pp. 2139–2152, Apr. 2017.

[14] S. Gao, X. Cheng, and L. Yang, "Generalized beamspace modulation for mmWave MIMO," in *Proc. IEEE Glob. Commun. Conf.*, 2018, pp. 1–6.

[15] S. Gao, X. Cheng, and L. Yang, "Spatial multiplexing with limited RF chains: Generalized beamspace modulation (GBM) for mmWave massive MIMO," *IEEE J. Sel. Areas Commun.*, vol. 37, no. 9, pp. 2029–2039, Sep. 2019.

[16] S. Guo, H. Zhang, P. Zhang, P. Zhao, L. Wang, and M. -S. Alouini, "Generalized beamspace modulation using multiplexing: A breakthrough in mmWave MIMO," *IEEE J. Sel. Areas Commun*. vol. 37, no. 9, pp. 2014–2028, Sep. 2019.

[17] Y. Fan, S. Gao, X. Cheng, L. Yang, and N. Wang, "Wideband generalized beamspace modulation (wGBM) for mmWave massive MIMO over doubly-selective channels," *IEEE Trans. Veh. Technol.*, vol. 70, no. 7, pp. 6869–6880, Jul. 2021.

[18] L. He, J. Wang, and J. Song, "On generalized spatial modulation aided millimeter wave MIMO: Spectral efficiency analysis and hybrid precoder design," *IEEE Trans. Wireless Commun.*, vol. 16, no. 11, pp. 7658–7671, Nov. 2017.

[19] L. He, J. Wang, and J. Song, "Spatial modulation for more spatial multiplexing: RF-chain-limited generalized spatial modulation aided MM-Wave MIMO with hybrid precoding," *IEEE Trans. Commun.*, vol. 66, no. 3, pp. 986–998, Mar. 2018.

[20] Y. Ding, V. Fusco, A. Shitvov, Y. Xiao, and H. Li, "Beam index modulation wireless communication with analog beamforming," *IEEE Trans. Veh. Technol.*, vol. 67, no. 7, pp. 6340–6354, Jul. 2018.

[21] Y. Cui, X. Fang, and L. Yan, "Hybrid spatial modulation beamforming for mmWave railway communication systems," *IEEE Trans. Veh. Technol.*, vol. 65, no. 12, pp. 9597–9606, Dec. 2016.

[22] P. Liu, M. Di Renzo, and A. Springer, "Line-of-sight spatial modulation for indoor mmWave communication at 60 GHz," *IEEE Trans. Wireless Commun.*, vol. 15, no. 11, pp. 7373–7389, Nov. 2016.

[23] N. Ishikawac, R. Rajashekar, S. Sugiura, and L. Hanzo, "Generalized-spatial-modulation-based reduced-RF-chain millimeter-wave communications," *IEEE Trans. Veh. Technol.*, vol. 66, no. 1, pp. 879–883, Jan. 2017.

[24] P. Liu, J. Blumenstein, N. S. Perovic, M. Di Renzo, and A. Springer, "Performance of generalized spatial modulation MIMO over measured 60 GHz indoor channels," *IEEE Trans. Commun.*, vol. 66, no. 1, pp. 133–148, Jan. 2018.

[25] N. Ishikawa et al., "Differential-detection aided large-scale generalized spatial modulation is capable of operating in high-mobility millimeter-wave channels," *IEEE J. Sel. Topics Signal Process.*, vol. 13, no. 6, pp. 1360–1374, Oct. 2019.

[26] A. Younis, N. Abuzgaia, R. Mesleh, and H. Haas, "Quadrature spatial modulation for 5G outdoor millimeter–wave communications: Capacity analysis," *IEEE Trans. Wireless Commun.*, vol. 16, no. 5, pp. 2882–2890, May 2017.

[27] S. Y. Nusenu and S. Huaizong, "Green secure communication range-angle focusing quadrature spatial modulation using frequency modulated diverse retrodirective array for mmWave wireless communications," *IEEE Trans. Veh. Technol.*, vol. 68, no. 7, pp. 6867–6877, Jul. 2019.

[28] J. Zhu, P. Yang, Y. Xiao, X. Lei, and Q. Chen, "Low RF-complexity receive spatial modulation for millimeter-wave MIMO communications," *IEEE Commun. Lett.*, vol. 22, no. 7, pp. 1338–1341, Jul. 2018.

[29] N. S. Perović, P. Liu, M. Di Renzo, and A. Springer, "Receive spatial modulation for LOS mmWave communications based on TX beamforming," *IEEE Commun. Lett.*, vol. 21, no. 4, pp. 921–924, Apr. 2017.

[30] S. Luo, X. T. Tran, K. C. Teh, and K. H. Li, "Adaptive spatial modulation for uplink mm-Wave communication systems," *IEEE Commun. Lett.*, vol. 21, no. 10, pp. 2178–2181, Oct. 2017.

[31] P. Yang, Y. Xiao, Y. L. Guan, Z. Liu, S. Li, and W. Xiang, "Adaptive SM-MIMO for mmWave communications with reduced RF chains," *IEEE J. Sel. Areas Commun.*, vol. 35, no. 7, pp. 1472–1485, Jul. 2017.

[32] S. Luo, P. Yang, Y. L. Che, and K. Wu, "Space-domain index modulation for mmWave cloud radio access networks," *IEEE Trans. Veh. Technol.*, vol. 69, no. 6, pp. 6215–6229, Jun. 2020.

[33] S. Luo, P. Yang, Y. L. Che, K. Wu, Y. Peng, and S. Li, "Generalized space domain index modulation for mmWave distributed antenna systems," *IEEE Trans. Veh. Technol.*, vol. 69, no. 11, pp. 14067–14071, Nov. 2020.

[34] O. Y. Kolawole, S. Vuppala, and T. Ratnarajah, "Multiuser millimeter wave cloud radio access networks with hybrid precoding," *IEEE Syst. J.*, vol. 12, no. 4, pp. 3661–3672, Dec. 2018.

[35] L. Bai, T. Li, Q. Yu, J. Choi, and W. Zhang, "Cooperative multiuser beamforming in mmWave distributed antenna systems," *IEEE Trans. Veh. Technol.*, vol. 67, no. 12, pp. 12394–12397, Dec. 2018.

[36] D. Yue and H. H. Nguyen, "Multiplexing gain analysis of mmWave massive MIMO systems with distributed antenna subarrays," *IEEE Trans Veh. Technol*,, vol. 68, no. 11, pp. 11368–11373, Nov. 2019.

[37] K. Satyanarayana, M. El-Hajjar, P. Kuo, A. A. M. Mourad, and L. Hanzo, "Adaptive transceiver design for C-RAN in mmWave communications," *IEEE Access*, vol. 6, pp. 16770–16782, 2018.

[38] A. K. Gupta, J. G. Andrews, and R. W. Heath, "Macrodiversity in cellular networks with random blockages," *IEEE Trans. Wireless Commun.*, vol. 17, no. 2, pp. 996–1010, Feb. 2018.

[39] Z. Pi and F. Khan, "An introduction to millimeter-wave mobile broadband systems," *IEEE Commun. Mag.*, vol. 49, no. 6, pp. 101–107, Jun. 2011.

[40] T. Bai and R. W. Heath, "Coverage and rate analysis for millimeter-wave cellular networks," *IEEE Trans. Wireless Commun.*, vol. 14, no. 2, pp. 1100–1114, Feb. 2015.

[41] G. Lee, Y. Sung, and J. Seo, "Randomly-directional beamforming in millimeter-wave multiuser MISO downlink," *IEEE Trans. Wireless Commun.*, vol. 15, no. 2, pp. 1086–1100, Feb. 2016.

[42] Q. Gao, X. Zhang, and J. Li, "Power control of V-BLAST system with per-antenna power constraints," *IEEE Commun. Lett.*, vol. 11, no. 11, pp. 833–835, Nov. 2007.

[43] Z. Wang and L. Vandendorpe, "Power allocation for energy efficient multiple antenna systems with joint total and per-antenna power constraints," *IEEE Trans. Commun.*, vol. 66, no. 10, pp. 4521–4535, Oct. 2018.

[44] M. Medra and T. N. Davidson, "Low-complexity robust MISO downlink precoder design with per-antenna power constraints," *IEEE Trans. Signal Process.*, vol. 66, no. 2, pp. 515–527,Jan. 2018.

[45] C. Chen, "MSE-based precoder designs for transmitter-preprocessing-aided spatial modulation under per-antenna power constraints," *IEEE Trans. Veh. Technol.*, vol. 66, no. 3, pp. 2879–2883, Mar. 2017.

[46] P. Yang, Y. Xiao, M. Xiao, J. Zhu, S. Li, and W. Xiang, "Enhanced receive spatial modulation based on power allocation," *IEEE J. Sel. Topics Signal Process.*, vol. 13, no. 6, pp. 1312–1325, Oct. 2019.